ADVANCING EARTH AND SPACE SCIENCE

JGR Space Physics

RESEARCH ARTICLE
10.1029/2020JA028917

**Key Points:**
- Characteristics of remote reconnection are inferred from multipoint observations of fields and particles at plasma sheet boundary layer
- Short-lived parallel-electric field disturbances accompanied by energy dispersed electrons are the first observables of remote reconnection
- Estimated reconnection electric field using remote sensing methods was 1.6~2.5 mV/m, which decreased to ~0.8 mV/m within ~20 s

**Supporting Information:**
- Supporting Information S1

**Correspondence to:**
R. Nakamura,
rumi.nakamura@oeaw.ac.at

**Citation:**
Wellenzohn, S., Nakamura, R., Nakamura, T. K. M., Varsani, A., Sergeev, V. A., Apatenkov, S. V., et al. (2021). Remote sensing of magnetic reconnection in the magnetotail using in situ multipoint observations at the plasma sheet boundary layer. *Journal of Geophysical Research: Space Physics*, *126*, e2020JA028917. https://doi.org/10.1029/2020JA028917

Received 12 NOV 2020
Accepted 15 DEC 2020

# Remote Sensing of Magnetic Reconnection in the Magnetotail Using In Situ Multipoint Observations at the Plasma Sheet Boundary Layer

**S. Wellenzohn[1,2], R. Nakamura[1], T. K. M. Nakamura[1,2], A. Varsani[1], V. A. Sergeev[3], S. V. Apatenkov[3], J. C. Holmes[1,4], E. E. Grigorenko[5], J. L. Burch[6], B. L. Giles[7], and R. B. Torbert[6,8]**

[1]Space Research Institute, Austrian Academy of Sciences, Graz, Austria, [2]Institute of Physics, University of Graz, Graz, Austria, [3]Earth's Physics Deptartment, St. Petersburg State University, St. Petersburg, Russia, [4]Los Alamos National Laboratory, Los Alamos, NM, USA, [5]Space Research Institute, Russian Academy of Sciences, Moscow, Russia, [6]Space Science and Engineering, Southwest Research Institute, San Antonio, TX, USA, [7]Goddard Space Flight Center, NASA, Greenbelt, MD, USA, [8]Space Science Center, University New Hampshire, Durham, NH, USA

**Abstract** Characteristics of the reconnection region are examined based on Magnetospheric Multiscale (MMS) observation of a plasma sheet boundary layer crossing on July 12, 2018 when both high-energy (>few keV) electrons as well as ions flowing parallel to the magnetic field showed distinct energy dispersion. Remote sensing techniques are applied to estimate location of reconnection region and injection time of these particles. The reconnection region is estimated to be located at $X = (-23 \pm 1.9)$ $R_E$ from electrons, comparable to that from ions, $X = (-24.5 \pm 0.7)$ $R_E$ by taking into account the time of flight effect as well as the effect of separatrix motion relative to the plasma. The electron injection times precede that of ions by ~6 s. We found that the time dispersed energetic electron beams away from X-line are accompanied by short-lived high-frequency parallel-electric field disturbances around plasma frequency. These wave packets are the first observable remote feature of reconnection. Using multi-point measurements of high energy ions, electrons, magnetic field, and parallel-electric field disturbances, reconnection electric field is estimated as 1.6–2.5 mV/m initially and decrease to ~0.8 mV/m within ~20 s. This study shows that the remote sensing scheme is an alternative method to infer the temporal/spatial changes of the magnetotail reconnection.

**Plain Language Summary** Magnetic reconnection is a process in which magnetic field energy is converted to particle energy in association with a change of the topology of the magnetic field in a small region smaller than the plasma particles can complete its gyration. Although the reconnection region is small, the effect of the outflowing particles from reconnection can be detected remotely. We study the remote effects of magnetic reconnection based on an observation by the four Magnetospheric Multiscale (MMS) spacecraft on July 12, 2018. Based on the energy and species dependent features and difference among the spacecraft, we deduced the characteristics of the remote reconnection such as the reconnection rate and its evolution.

## 1. Introduction

Plasma sheet boundary layer (PSBL) is the main channel for mass and energy transport in the magnetotail (e.g., Grigorenko et al., 2011, and reference therein). A spacecraft traveling equatorward from lobe to plasma sheet first encounters electrons streaming parallel along magnetic field line then enters regions with high-energy ion beams (Parks et al., 1998; Takahashi et al., 1988). High energy PSBL beams contain energy dispersed signatures, meaning that particles having different energies are observed at different locations or times. Onsager et al., (1990) showed how the levels of low speed cut-offs for earthward and tailward flowing electrons parallel to the magnetic field change as spacecraft traverses from lobe to PSBL and suggested that these signatures are due to time of flight (ToF) effect of different particles injected from the reconnection region. There are mainly two types of dispersed structures found in the ion beams: time-dispersed-structure (TDS) and the velocity-dispersed-structure (VDS), originally named for observation from low-altitude ion beam features that are connected to PSBL (e.g., Sauvaud & Kovrazhkin, 2004). These dispersed signatures give information about acceleration processes in the equatorial plasma sheet associated with magnetic reconnection (Delcourt et al., 1999; V. A. Sergeev et al., 2000). Reconnection drives accelerated plasma beams, which spread along the magnetic field lines due to ToF effect leading to TDS (Sauvaud et al., 1999). Injected particles drift also perpendicular to magnetic field due to E × B velocity, usually toward the plasma sheet center. Since slower particles take longer time to reach the spacecraft, this motion leads a spatial (latitudinal) dispersion due to a velocity filter (VF) effect, which is called also VDS.

While earlier studies on high-energy beam observations at PSBL related to TDS have been limited for ions (e.g., Sauvaud et al., 1999), Varsani et al. (2017) for the first time reported electron energy dispersion that can be interpreted as due to TDS together with ion energy dispersion in a PSBL crossing event. The event took place during a storm-time substorm on June 23, 2015, when some of high time-resolution particle measurements onboard Magnetospheric Multiscale (MMS) were already operating in spite of MMS still being in the commissioning phase. By assuming the dispersion to be due to ToF effect of the particle beams accelerated at the active reconnection region, the X-line location was then estimated. The obtained location, that is, 16–18 $R_E$ downtail, was comparable to the estimated values from DMSP low-altitude observation of energy dispersion of ions and electrons.

Another important parameter one can infer from the separatrix observations is the reconnection rate. A method to estimate the reconnection rate using multi spacecraft data of parallel electron beam (or associated field-aligned current) at the separatrix region was proposed by T. K. M. Nakamura et al. (2018a). The method was validated using data from PIC simulation of reconnection. In this method, the reconnection rate is obtained from the speed of separatrix boundary. The boundary motion needs to be obtained independent of plasma motion and therefore requiring multi-point measurement. T. K. M. Nakamura et al. (2018a) applied this methods to an outer plasma sheet dipolarization event observed by MMS in the near-Earth region (X > −6 RE) studied by R. Nakamura et al. (2018). Although electron beam signatures were not clear due to preexisting plasma sheet component for this event, magnetic field disturbance expected from field-aligned current could be used for the analysis to obtain a reconnection electric field, $Er \sim 15$ mVm.

In this study, we examine detail particle and field signatures observed by the four MMS spacecraft during a PSBL crossing on July 12, 2018 associated with a small substorm intensification. During this interval all the MMS instruments were in burst (high-time resolution) mode and energy dispersion both in electron and ion were detected. We extend and apply the above mentioned remote-sensing methods using multi-point measurement of different disturbances including ions, electrons, and electric and magnetic fields. Signatures associated with the arrival of the different disturbances from the remote reconnection site are examined to obtain characteristics of the reconnection site including location, timing, and reconnection rate. While this study, concentrate mainly on the quick disturbances associated with electron beam dynamics around electron boundary layer (EBL), remote reconnection signatures deduced from ions and associated Hall-type field disturbance are shown by Sergeev et al. (2020) based on nine MMS PSBL crossing events including the one discussed in this study.

## 2. Event Overview

On July 12, 2018 07:00–09:00 UT MMS four spacecraft were located at (−17.5, 1.6, 5.8) $R_E$ (Figure 1a) in the northern lobe/plasma sheet boundary during a weak westward electrojet enhancement of about −300 nT (Figure 1b). The ion and electron omni directional spectra (Figures 1c and 1d) are obtained from the Fast Plasma Instruments (FPI) (Pollock et al., 2016) and the magnetic field from the Flux Gate Magnetometer (FGM) (Russell et al., 2016). MMS was initially located in the lobe with low-energy electrons, typical for polar rain. A sudden encounter of the PSBL takes place due to the plasma sheet expansion associated with the second weak electrojet activation at around 08:00 UT (Figure 1b) indicated by the vertical line. The plasma sheet expansion was accompanied by enhanced Bz (Figure 1e), a feature of a dipolarization, and enhanced ion flows (Figure 1f). During the whole PSBL crossing period from 08:01:37 to 08:03:35 several step-like enhancements of $B_Z$ and fluctuations of $B_Y$ indicating field aligned currents (FAC) were observed. These stepwise $B_Z$ enhancements and predominant FAC signatures have been reported as characteristic of dipolarization in the PSBL region (R. Nakamura et al., 2018). This study focuses on the initial signature of the PSBL crossing as shown in the right panels in Figure 1.

10.1029/2020JA028917

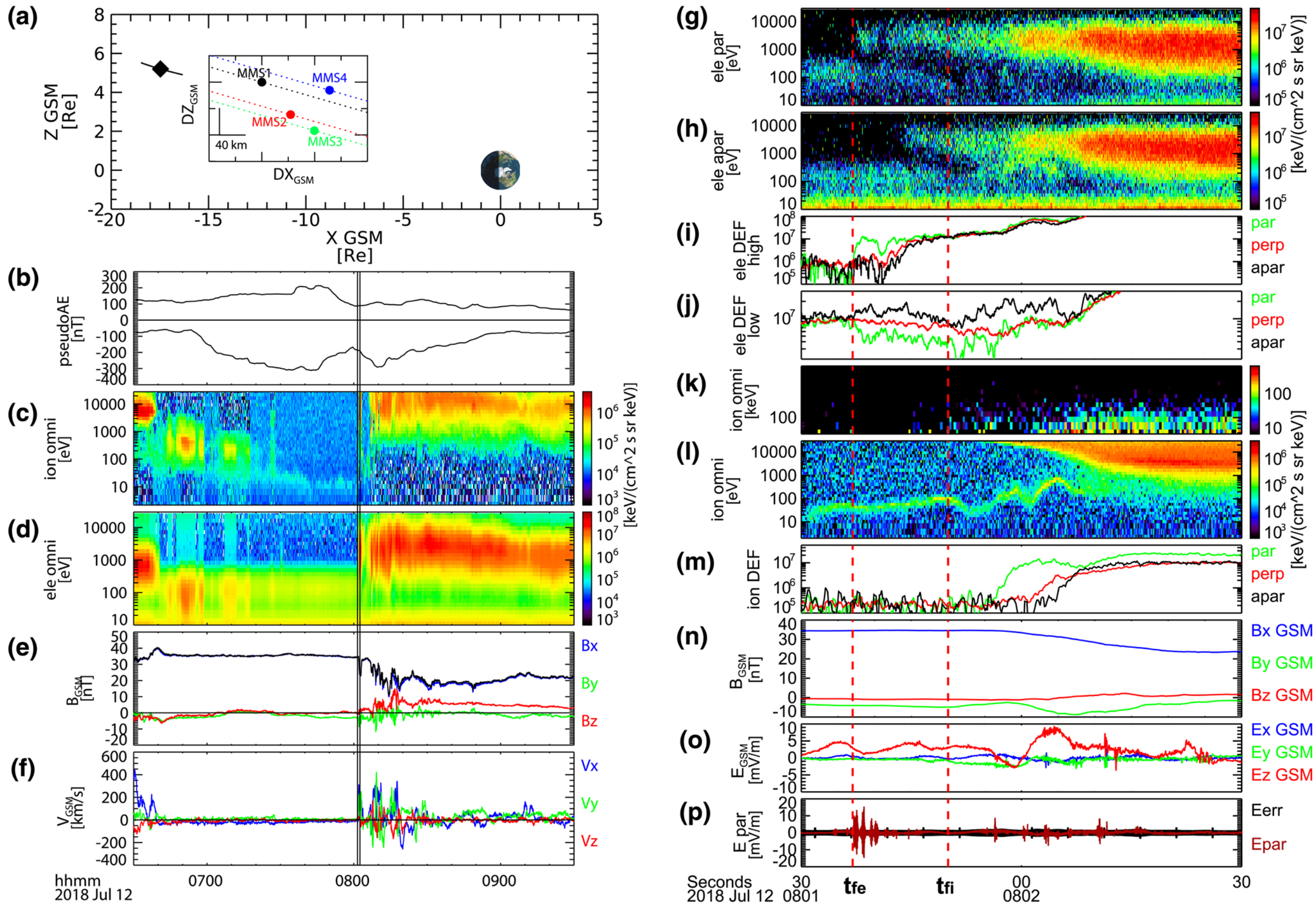


**Figure 1.** MMS observation of the PSBL crossing on July 12, 2018. (a) Orbit in the X-Z plane in GSM coordinate system with the location of MMS at 08:00 UT and the relative location of the four spacecraft. (b) Pseudo AE obtained from THEMIS ground-based network. Omnidirectional energy spectra from ion (c and d) electron measured by FPI. (e) Magnetic field, (f) bulk ion velocity, energy spectra for (g) parallel and (h) anti-parallel electrons. Differential energy flux (DEF) of parallel (green), perpendicular (red), and antiparallel (blue) electrons with energy between (i) 0.7–30 keV and (j) 30–500 eV. Omnidirectional ion energy spectra: (k) above 45 keV measured by FEEPS and (l) below 30 keV measured by FPI. (m) DEF of ions in the energy range from 0.7 to 30 keV with the same color scheme as (i). (n) Magnetic field and (o) electric field in GSM coordinate and (p) electric field component parallel to the magnetic field. The red vertical lines mark the injection onset time of high energy parallel electrons ($t_{fe}$) and that of high-energy parallel ions ($t_{fi}$).

At 08:01:37 ($t_{fe}$) MMS1 observed earthward moving high-energy (>1 keV) anisotropic electrons (Figure 1g). This is followed by enhancement in tailward (antiparallel) traveling component together with perpendicular plasma sheet electrons at 08:01:44 (Figures 1h and 1i). Enhancements in high-energy ions, also earthward moving with energy dispersion (Figures 1l and 1m), started later in conjunction with more isotropic electrons (Figure 1i). This ion energy dispersion signature likely extended to energies of up to 100 keV (Figure 1k), measured by the Fly's Eye Energetic Particle Spectrometer (FEEPS) (Blake et al., 2016). Although the directional spectra cannot be calculated at a sufficient time resolution with FEEPS data, we may assume that the FEEPS ions are also directed earthward inferring from the anisotropy of FPI high-energy ions. The first ion dispersion signature took place therefore around 08:01:50 ($t_{fi}$). Similar sequences of the anisotropy observations by MMS in the electron and ion boundary layers have been reported by Varsani et al. (2017) in a PSBL crossing Earthward of reconnection region during a storm time substorm event. Similar to the event reported by Varsani et al. (2017), the observed ion jet is associated with positive Bz enhancement indicative of reconnection region at tailward of MMS. The initial enhancement of the Earthward (parallel) high-energy electrons (Figures 1g and 1i) therefore indicate the arrival of the accelerated and injected electrons along the separatrix of a reconnection region. The delay of the tailward (antiparallel) high-energy electron beams (Figures 1h and 1i) is expected to be due to the time that those injected electrons are bounced back from the mirror point closer to the Earth as well as due to the time it takes the spacecraft to encounter the field lines where such mirrored electrons are existing.

The energy of the narrow low-energy ion band, which can be seen in Figure 1l from the beginning of the plotted time interval, matches with those produced by a cold E x B drifting H+ ions supported also by composition measurements (not shown). At 08:02:07 the narrow cold ion band (few 10 to few 100 eV) started to mix with the high-energy ions as MMS entered the ion plasma sheet (Figure 1l) where anisotropy of high-energy electrons significantly diminished. The low-energy (<500 eV) electrons in the parallel spectra (Figure 1g) show typical signature of the polar rain electrons encountering an X-line as first reported by Shirai et al. (1997). The decrease in polar rain high-energy cutoff and resulting gap in the distribution suggests that polar rain electrons are accelerated at the X-line and thereby shifted to higher energies, reducing the flux of the earthward low-energy electrons. (Figures 1h and 1j).

A clear change in the magnetic field (Figure 1n) becomes visible only after the onset of the high energy ion event, $t_{ti}$. $B_X$ declines steadily from 34 to 24 nT, $B_Y$ decreases from −2 to −8 nT, while $B_Z$ sees a reversal from -2 nT to 1 nT associated with the dipolarization. While the 10s oscillation of electric field obtained by the double probe instrument (EDP) (Ergun et al., 2016; Lindqvist et al., 2016) (Figure 1o) in the lobe region is due to the wake effect of the positively charged spacecraft, there are some disturbances in the DC electric field associated with the expansion of the plasma sheet (discussed more detail in supporting information S1). The first signatures of the electric field, are however, the high-frequency parallel electric field waves (Figure 1p) around $t_{fe}$ when the high-energy electrons are detected. Such a high-energy electron beam associated with high-frequency waves has been predicted by Fujimoto and Machida (2006) in a simulation of magnetic reconnection at the separatrix region away from the X-line.

## 3. Location of the Reconnection Region

Figure 2a shows the electron inverse velocity spectra of the MMS1 for the parallel (Earthward) component around $t_{fe}$ (upper panel) and ions around $t_{fi}$ (lower panel). The vertical axis is the reciprocal speed of the particles, $v^{-1}$, in sec/$R_E$ units. The resolution of the plotted energy flux is 30 ms for electrons and 150 ms for ions, respectively. Both the electrons and ions show linear trends in the onset of the enhancement in the flux showing the energy dispersion features. Assuming the dispersion to be due to the ToF effect, that is, TDS, a linear fit of the onset times of the dispersion allows one to determine the distance traveled between the source region and the spacecraft, as has been performed for ions (e.g., Sauvaud et al., 1999) and electrons (Bai et al., 2019; Varsani et al., 2017). The injection time (time when the particles observed at the spacecraft had been injected into the separatrix region), $t_0$, can be then derived from the intersection of the dispersion fit with the horizontal axis, that is time when $v^{-1} \sim 0$ s/RE. Detailed analysis scheme is explained in the supporting information S1.

We determined the dispersion line by first binning the data to enhance the visibility of the signatures by removing the smaller scale disturbances. Here, we averaged over three (four) data points in time for ions (electrons), which translates to temporal bins of 450 ms for ions and 120 ms for electrons, respectively. Electron data are further averaged also over two energy (velocity) levels. The averaging still leaves at minimum six to eight energy levels for fitting. The white solid lines in Figure 2a show the result for the linear fit of the slope of the dispersion. The estimated source location, $L_{\mathrm{ToF}}$ (see the derivation scheme in supporting information S1), is shown in Figure 2b. For error estimation of this scheme, we estimated the effect of $\pm$ one bin time deviation in the maximum and minimum energy (i.e., inverse of the velocity) in the slope, and thereby obtained the error in estimating the distance of X-line. This error is presented as vertical bars in Figure 2b.

The observed plasma sheet expansion, which is expected to be caused by the enhanced reconnection process of lobe field lines (e.g., Sergeev et al., 2008), will result in also vertical motion of the reconnected flux tube. While the separatrix moves outward (+Z) as reconnection evolves, flux tube motion due to enhanced earthward/equatorward transport or current sheet flapping or plasma sheet reconfiguration can result in also vertical motion as visualized in Figure 2c for a case of equatorward (-Z) convection electric field. The diagram shows how the high-energy parallel electron and ion beams, which are originally produced near the X-line, travel along the reconnected field lines. The higher energy particles travel ahead of lower energy particles, leading to a ToF related energy dispersion. Yet, the observed reconnection signatures of slower particles, actually, are on older reconnected field lines such that the vertical distance to the source is larger due to equatorward E B convection. That is, in addition of ToF effects, movement perpendicular to the

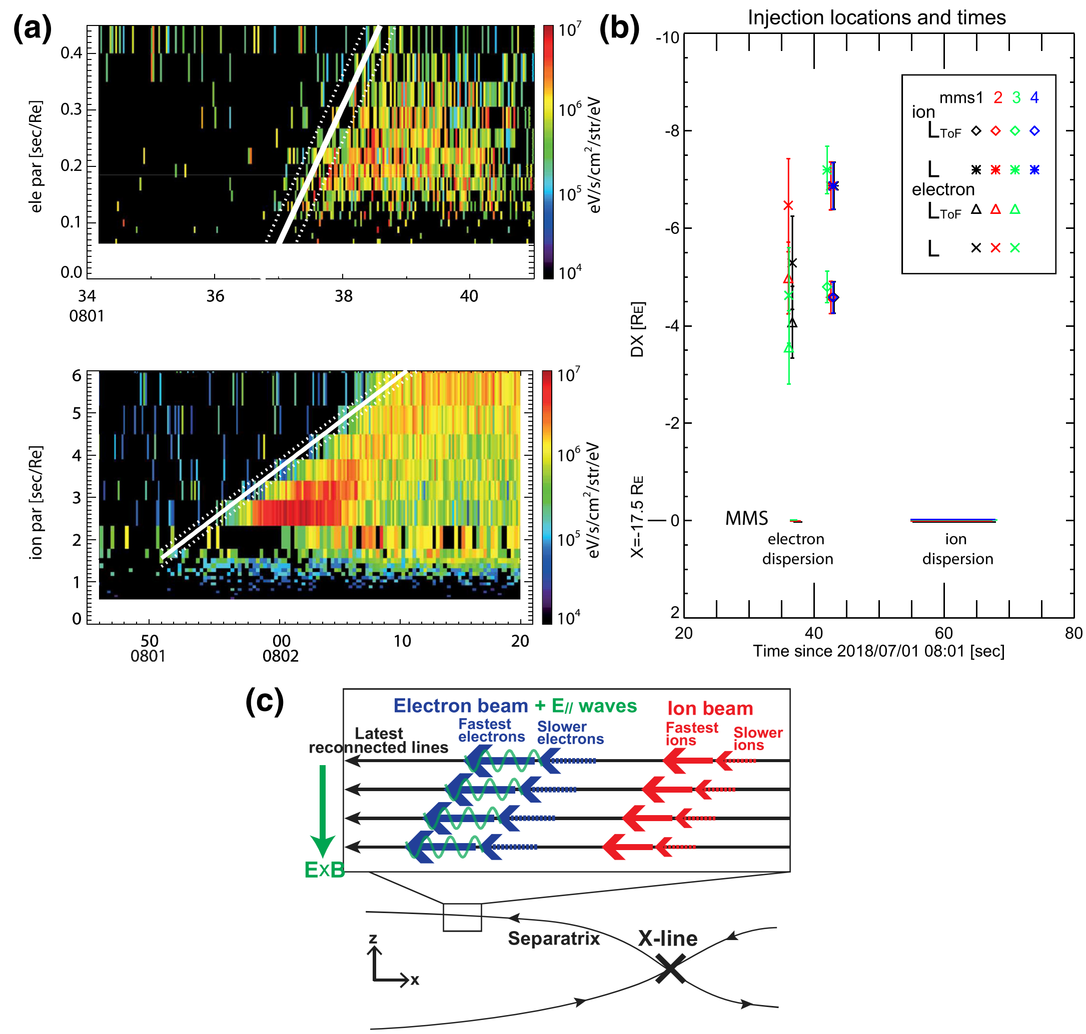


**Figure 2.** Observation of particle energy dispersion and its relationship to X-line. (a) Energy dispersion of earthward moving electrons (upper panel) and ions (lower panel) measured by FPI on MMS1. The linear fit of the dispersion is shown as solid white line, with dashed lines separated by two data bins. The bottom part of the ion spectra, below 2.3 s/RE, is the omnidirectional spectra measured by FEEPS not used in the fitting routine. (b) Time and location of the reconnection. The different symbols are plotted at the estimated injection time, $t_0$, and at the location of X-line relative to MMS (MMS1: black, MMS2: red, MMS3: green, and MMS4: blue) from the dispersion fit. The injection locations of ions (electrons) considering only the ToF effect, $L_{\mathrm{Tof}}$, are shown as diamonds (triangles) while those with corrections taking into account vertical motion, L, are show as asterisks (x). The vertical bars represent the 1-bin errors when calculating the energy dispersion line (see detail in the text). Time interval of ion and electron energy dispersion observed at MMS are also shown as horizontal bars at MMS location, DX = 0. (c) Schematic of typical reconnection signatures at a reconnection separatrix boundary region located sufficiently far from the X-line.

boundary needs to be taken into account. This effect has not been considered in previous studies when estimating the X-line location.

A correction due to the above convection effect can be added to the separatrix motion and the corrected distance to the injection region, $L$, is described as given in Equation 1 (see supporting information S1, Equation S5).

$$L = L_{\mathrm{ToF}}\left(\frac{V_T}{V_T - V_C}\right) = L_{\mathrm{ToF}} R_C \tag{1}$$

Here, $V_C$ and $V_T$ are the measured (spacecraft frame) convection velocity and the velocity of the separatrix and $Rc$ is the correction factor. We assume a 2D reconnection geometry where the separatrix is within the

$L$-$N$ plane and consider the $N$ component of $V_C$ and $V_T$, which is the normal component to the current sheet. The 2D assumption should be valid for this event, which has hardly no guide field (<0.1).

As described in supporting information S1, in this particular event, the normal direction was obtained as $\boldsymbol{N} = (-0.06, -0.255, 0.967)_{\mathrm{GSE}}$ using Tsyganenko 15 model (Tsyganenko & Andreeva, 2015). $V_C$ was calculated using FGM and EDP data. The separatrix velocity $V_T$ can be calculated from timing analysis of four-point observations (Harvey, 1998). Here we applied the method to the magnetic field data as has been successfully performed for MMS data in different areas of the magnetosphere (R. Nakamura et al., 2018; Plaschke et al., 2016). The resulting $V_T$ profile is shown in Figure S2. The timing velocity from the magnetic field could be reliably obtained when sufficient differences (~0.1 nT) exist among the spacecraft. Hence $V_T$ could be only determined after 08:01:50 UT when the magnetic disturbances associated with the plasma sheet expansion become identifiable. The average correction factor after 08:01:50 UT was estimated to be $R_C = 1.7$. As will be discussed in Section 3, $V_{\mathrm{T}}$ was possible to obtain from electron and electric field signatures around the time of electron energy dispersion observation, which give us a value of $R_C = 1.3$. For electrons we therefore used $R_C = 1.3$, while for ions we used the average of these two values, that is, $R_C = 1.5$.

The result of the estimated X-line location and the injection times taking into account the convection effects as well as the bin-errors described above for different spacecraft, ions and electrons are shown in Figure 2b. The averaged radial distance of the injection location using electron observations of MMS1, MMS2, and MMS3 (MMS4 was not able to provide electron distributions in burst mode for this event) was $L_{\mathrm{ToF}} = (4.2 \pm 1.5)\ R_E$ and $L = (5.5 \pm 1.9)\ R_{\mathrm{E}}$. We obtained comparable distances from the ion dispersion of all the four spacecraft: $L_{\mathrm{ToF}} = (4.6 \pm 0.4)\ R_E$ and $L = (7.0 \pm 0.7)\ R_E$. The larger variation in distance for electrons is somewhat expected since their velocity is more than an order of magnitude higher than that of the ions. On the other hand, effect of the convection correction is more significant for ion case, due to the longer traveling time, equivalent to larger distance. The electron injection time was estimated from ToF as $t_0 = (08{:}01{:}36.3 \pm 0.5)\ s$. The ion injection time was estimated to be $t_0 = (08{:}01{:}42.7 \pm 0.9)\ s$, which is about 6 s later than electrons. Such delay in the ion injections relative to the electron injections was also reported by Varsani et al. (2017).

## 4. Reconnection Rate

Another important application of the remote sensing observation is to estimate the reconnection electric field, $E_r$, from the motion of the separatrix and the plasma convection. The validity of the method was proven based on application of the method to data from a PIC simulation of reconnection (T. K. M. Nakamura et al., 2018a). $E_r$ can be estimated at the reconnection separatrix region as:

$$E_r \sim \left[\left(\boldsymbol{V}_{\mathbf{sep}} - \boldsymbol{V}_{\mathbf{c}}\right), \times, \boldsymbol{B}\right]_M \tag{2}$$

$\boldsymbol{V_C}$ is the $\boldsymbol{E} \times \boldsymbol{B}$ drift velocity and $\boldsymbol{V}_{\mathbf{sep}}$ is the separatrix velocity. T. K. M. Nakamura et al., (2018a) showed that instead of $\boldsymbol{V}_{\mathbf{sep}}$ itself, one can calculate from the two spacecraft timing velocity as long as the separation distance of the spacecraft within the separatrix plane is sufficiently small compared to the distance that the signal of interest can propagate within the temporal difference. Here we used timing velocity, $\boldsymbol{V_T}$, using particle and field disturbances from the four MMS spacecraft. For the orientation of the separatrix plane, we used the normal direction, $\boldsymbol{N}$, given in Section 3. Using simulation data of magnetic field disturbance, T. K. M. Nakamura et al. (2018a) showed that timing velocity from two spacecraft and velocity obtained from four spacecraft provide comparable reconnection rate as long as the above condition is fulfilled. In the following, we first examine the initial signatures of the particles and fields among the different spacecraft and we then obtain $E_{\mathrm{r}}$ using different disturbances observed by multiple spacecraft.

Figures 3a–3f show the electron spectra and the parallel electric field from the three spacecraft, MMS1, MMS2, and MMS3. As mentioned in Section 2, MMS detected enhanced E|| waves associated with the TDES (electron TDS). The frequency of the waves is in a range of electron plasma frequency (Figure S3c) and are likely electron beam driven Langmuir waves as an indication of TDES arrival such as those discussed by Fujimoto and Machida (2006). Note that while parallel component of >keV electrons are present almost

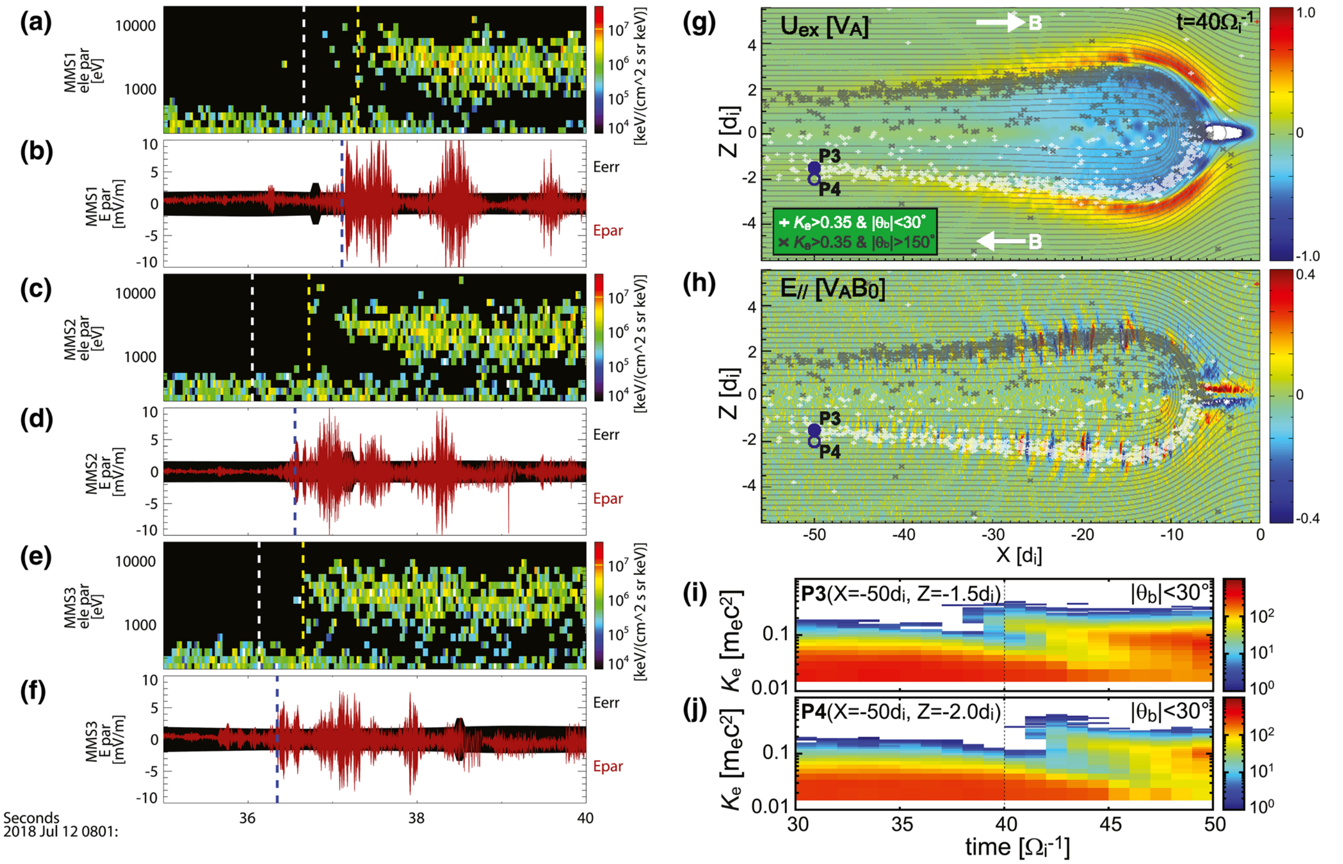


**Figure 3.** Observed and simulated separatrix signatures used for the estimation of the reconnection rate $E_r$. TDS of earthward moving electrons and parallel electric field measured by (a and b) MMS1, (c and d) MMS2 and (e and f) MMS3. The onset timings of the first significant (|E| > 3 mV/m) electric field fluctuations, the estimated onset of TDS, $t_{0e}$, and the onset of 6 keV (0.14 s/Re) electron flux enhancement are shown with blue, white, and yellow lines. (g) X-component of the electron bulk velocity $U_{ex}$ and (h) electric field component parallel to the magnetic field, $E_{//}$, from 2-D fully kinetic simulation of the anti-parallel reconnection (T. K. M. Nakamura et al., 2018a) for the negative outflow velocity side at $t = 40\Omega_i^{-1}$. The white and gray marks in (g and h) show the locations of parallel (pitch angle $|\theta_b| < 30°$) and anti-parallel ($|\theta_b| > 150°$) moving electrons with their kinetic energy, $K_e > 1.4\ m_e V_{Ae}^2$, where $V_{Ae}$ is the electron Alfven speed. Virtual observations of energy spectrograms for parallel ($|\theta_b| < 30°$) moving electrons at location (i) P3 and (j) P4 shown in (g) and (h). (P3 and P4 are from the same probes shown in Figures 3g and 3i in T. K. M. Nakamura et al. (2018a)).

continuously after $t_{fe}$ during the PSBL crossing (Figures 1g and 1i), significant wave activity is only observed at the beginning of the interval (Figure 1p). Figures S3a and S3b compare reduced electron distributions sampled during and shortly after the wave packet observations. In the former case, an electron beam was likely driving the observed parallel electrostatic waves. In the latter case, however, higher energy electrons appear as a nearly isotropic shoulder, not likely to cause strong Langmuir turbulence. This suggests that on the latter case the electron beam may have already been dissipated before reaching MMS or is simply not present on that field line. This observation suggests therefore that the observed E|| wave packets can also be used as a signature of the electron beam arrival.

In order to confirm the relationship between the electron beams and the parallel electric field disturbances at the separatrix region at an active reconnection site, we examined parallel electric field profile using the same 2-1/2D PIC simulation of reconnection that was used to validate the method of reconnection rate estimation (T. K. M. Nakamura et al., 2018a). Since the initial condition of this simulation is not adjusted to any specific observation, we cannot compare quantitative values such as the reconnection rate. Instead, we examine how the electron beam is related to the disturbances in a distant separatrix region in a 2D reconnection setting, which is consistent with our event based on the low-guide field value as mentioned before. Figures 3g and 3h show 2D distribution of the electron flow and parallel electric field in the reconnection plane. Figures 3i and 3j show virtual observation of electron spectra at two location, P3 and P4, near the separatrix at far downstream of the reconnection jet, at about 50 $d_i$ away from the X-line, where $d_i$ is ion inertia length. The simulation results shown are from $t = 40\Omega_i^{1}$, where $\Omega_i$ is the ion cyclotron frequency. This corresponds to the time when high-energy electrons with energy higher than $E_e > 1.4\ m_e V_{Ae}^2 = (0.35\ m_e c^2)$ have reached the point labeled P3 but not P4. From the difference of the observation timings of the high-energy electrons at P3 and P4, T. K. M. Nakamura et al. (2018a), successfully estimated the reconnection rate and confirmed that the estimated rate agrees with the rate directly measured at the X-line. The X-line distance determined in the previous section indicates that MMS was located at about 56∼110 $d_i$ from the X-line, using the ion inertial length at ∼08:02 UT inside the current sheet for this event. This distance is comparable to that of the location of virtual measurements by P3 and P4, which represent observations near the separatrix region downstream of the reconnection jet region. The simulation indeed well recover the parallel profile of the electron spectra (Figures 3i and 3j) similar to the observation. It can be also seen in Figure 3h that the locations of the high-energy electrons are reasonably consistent with the locations where moderate strengths of E//waves were detected, confirming that the electron beams from reconnection site can excite the observed E//waves. Similar waves associated with the electron beam streaming out from reconnection site are reported also in the simulation results by Fujimoto and Machida (2006).

In order to deduce the reconnection electric field from these electron-associated disturbances, we used the timing velocity of the following three features: (1) The estimated electron injection time, $t_{0e}$, (2) the start time of E|| disturbances with amplitude |E| >3 mV/m, $t_{\mathrm{Epar}}$, and (3) the start time of TDS electrons, that is flux enhancement above 6 keV (0.14 s/$R_E$), $t_{\mathrm{TDES}}$. The out of reconnection plane direction, $\boldsymbol{M}$**,** is determined from $\boldsymbol{N} \times \boldsymbol{B_0}$, where $\boldsymbol{B_0} = (34.5, -3.7, -1.7)$ nT is an average magnetic field between 08:01:34-08:01:38 among all spacecraft. We used the average $\boldsymbol{V_C} = (8.6, 67.0, 27.6)$ km/s during the same interval. The timing velocity is determined using data from the three spacecraft assuming a planar boundary tangential to $\boldsymbol{B_0}$. This assumption will not affect the result, since we are only interested in the perpendicular component of the timing velocity (see Equation 2), but has an advantage to allow comparison of the different methods using data from the same spacecraft. The estimated separatrix velocity perpendicular to $\boldsymbol{B_0}$ would then be (1) $\boldsymbol{V_T}= (-2.0, -50.1, 67.5)$ km/s, (2) $\boldsymbol{V_T}= (1.1, -14.2, 53.3)$ km/s, (3) $\boldsymbol{V_T}= (0.5, -25.2, 63.2)$ km/s. The estimated reconnection electric field, $E_r$ is then (1) 2.4 mV/m, (2) 1.6 mV/m, and (3) 2.0 mV/m, respectively.

We also tried to estimate $E_r$ from TDIS (ion TDS). To minimize the error due to the assumption of constant velocity over all the time between particle injection and observation, we used the timing of the start time of TDIS. That is, we use the start time of >28 keV ions, instead of the estimated $t_{0i}$ from the energy dispersion for determining the timing velocity. Using average magnetic field and convection velocity between 08:01:55 and 08:01:56 UT, $\boldsymbol{V_C} = (5.2, 22.2, 56.6)$, $\boldsymbol{B_0} = (34.6, -2.8, -2.0)$ nT, and using the estimated timing velocity, $\boldsymbol{V_T}= (-85.4, -114.1, 98.9)$ km/s, we obtain $E_r = 2.5$ mV/m which is comparable to those from TDES.

$V_T$ from magnetic field disturbances also provides motion of the boundary during most of the TDIS time as can be seen in Figure S2. At 08:01:50 (near the start of energetic proton observation) $V_C$ ∼23 km/s, $V_T$ ∼89–94 km/s. At 08:02:00 (in the later part of observed proton energy dispersion) $V_C$ ∼55 km/s, $V_T$ ∼77–78 km/s. For $B = 34$ nT these differences results in reconnection rates $E_r = 2.3$ mV/m and 0.8 mV/m, accordingly.

## 5. Summary and Discussion

We showed that both electron and ion energy dispersions observed during the PSBL crossing on July 12, 2018 can be interpreted to be formed associated with remote reconnection. Its average location from the three MMS1, MMS2, and MMS3 observations was estimated to be $X = (-23.0 \pm 1.9)\ R_E$ for electrons and a comparable distance from the four MMS spacecraft, $X = (-24.5 \pm 0.7)\ R_E$, was obtained for ion, by also determining the separatrix motion relative to the ambient plasma from multi-point data analysis. These are locations typical of the near-Earth neutral line obtained from previous studies (Nagai et al., 2005, and reference therein). Consistent locations between ions and electrons, but an injection region at X = -16 ∼-18 $R_E$, has been obtained by Varsani et al. (2017), which was estimated by the ToF effect only. Since the results of estimating the X-line location using electrons was less sensitive to the additional effect from ambient plasma motion as we showed in this study, the near-Earth location obtained by Varsani et al., (2017) is most likely due to the storm-time substorm condition where the thin current sheets are expected to form closer to Earth. Similar to Varsani et al. (2017), the obtained injection time of the electrons was earlier (by ∼6s) than that of ions, which may suggest different acceleration time-scales between ions and electrons. From the comparison among the different spacecraft, we can conclude that the estimation of the location of injection for ions shows more stable results among different spacecraft compared to electrons, but it is more affected by the ambient plasma motion (convection). On the other hand, the time of the injections estimated from the electrons are more stable than that from ions.

Onsager et al. (1990) introduced a method to obtain X-line location using the low speed cut-off of the Earthward and tailward parallel velocity distribution. In this study, however, dispersion of electron beam was detected only for Earthward beam before entering the plasma sheet with isotropic distribution. That is, MMS did not observe a region of bi-directional parallel velocity distribution as shown by Onsager et al (1990). The difference may come from the transient and localized feature related to activation of reconnection discussed in this study, whereas the changes in the bi-directional parallel distribution profile discussed by Onsager et al. (1990) are profiles due to a longer time-scale (∼4 min) PSBL crossing and are related to signature due to VDS, that is spatial profile due to velocity filter effect.

Another important feature that accompanies the time dispersed electrons is the short-lived, parallel-electric field disturbances around the electron plasma frequency, as reported in past kinetic simulation studies (Fujimoto & Machida, 2006) and as also shown in the PIC simulation (Figure 3). This parallel wave signature was found to be the first remotely observable signature of reconnection during the separatrix crossing.

The reconnection electric field values obtained from the separatrix motion using timing velocity of electrons TDS and the E|| waves were $Er = 1.6–2.4$ mV/m. These values are comparable to $Er = 2–3$ mV/m, which was estimated remotely as well as directly around the electron diffusion region (T. K. M. Nakamura et al., 2018b) during a small substorm (AE∼200 nT) on July 11, 2017. One order of magnitude higher Er (∼15 mV/m) was obtained using the same method applied to another PSBL crossing during an intense substorm (AE∼1,000 nT) (T. K. M. Nakamura et al., 2018a). A more statistical approach on the PSBL signatures would be needed to investigate the relation between the local reconnection physics to the global geomagnetic activities. This study newly confirmed that both the electron energy dispersions and the E|| waves during the PSBL crossing are useful signatures to remotely estimate the reconnection rate.

We also applied the same remote sensing technique to the slower propagating boundary disturbances, that is, the magnetic field and ion energy dispersions. Note that the remote sensing method assumes that reconnection signatures travel along the boundary much faster than the motion of the boundary in the perpendicular direction. The boundary motion speed during this event is on the order of 100 km/s at maximum (Figure S2). The parallel electron velocity is on the order of V|| ∼ $10^{4\text{-}5}$ km/s, while for ions it is on the order of V||∼1,000 km/s (i.e., only one order of magnitude higher than the boundary motion speed) and low frequency magnetic field disturbances likely propagate at about the Alfven speed, ∼5,000 km/s. In addition, this technique also assumes constant $E_r$ and convection velocities during characteristic observations. The time scale for electron TDS, 1.5 s, and ion TDS, 20 s indicate that application to ions needs some caution in particular when using the lower energy part. Nonetheless, $E_r$ ∼2.5 mV/m obtained from timing of high-energy ions (>28 keV) and $E_r$ ∼2.3 mV/m obtained from magnetic signatures around the onset of ion TDS are quite consistent with those obtained from electrons. As shown in Figure S2 the estimated $E_r$ decrease to $E_r$ ∼0.8 mV/m by the end of ion TDS suggests that there is variation of the reconnection rate in the time-scale of ∼20s, which corresponds to $\sim 10\Omega_i^{-1}$ (for 34 nT). Combining these different initial disturbances of TDS therefore provide information also on the temporal evolution of remote reconnection site. Since the separatrix region is extended in a wide region, probability of its crossing by spacecraft is expected to be much higher than the spacecraft encounter of the reconnection site, our study shows that combination of different remote sensing schemes applied to different data set can be an alternative method to determine the temporal/spatial characteristics of magnetotail reconnection.

## Data Availability Statement

The MMS data are publically available from Science Data Center at CU/LASP (https://lasp.colorado.edu/mms/sdc/public/). Ground based pseudo AE data are available from THEMIS data directory (http://themis.ssl.berkeley.edu/data/themis/thg/).

**Acknowledgments**

This work was supported by the Austrian Science Fund (FWF): I2016-N20, I3506-N27, P32175-N27 and by the Austrian Research Promotion Agency (FFG): 873685 and by RSF grant 18-47-05001.

## References

Bai, S.-C., Shi, Q., Zong, Q.-G., Wang, X., Tian, A., Degeling, A. W., et al. (2019). Electron dispersion and parallel electron beam observed near the separatrix. *Journal of Geophysical Research: Space Physics*, *124*, 7494–7504. https://doi.org/10.1029/2019JA026836

Blake, J. B., Mauk, B. H., Baker, D. N., Carranza, P., Clemmons, J. H., Craft, J., et al. (2016). The Fly's Eye Energetic Particle Spectrometer (FEEPS) Sensors for the Magnetospheric Multiscale (MMS) Mission. *Space Science Reviews*, *199*, 309–329. https://doi.org/10.1007/s11214-015-0163-x

Delcourt, D. C., Dubouloz, N., Sauvaud, J.-A., & Malingre, M. (1999). On the origin of sporadic keV ion injections observed by Interball-Auroral during the expansion phase of substorms. *Journal of Geophysical Research*, *104*(24), 929.

Ergun, R. E., Holmes, J. C., Goodrich, K. A., Wilder, F. D., Stawarz, J. E., Eriksson, S., et al. (2016). Magnetospheric Multiscale observations of large-amplitude, parallel, electrostatic waves associated with magnetic reconnection at the magnetopause. *Geophysical Research Letters*, *43*, 5626–5634. https://doi.org/10.1002/2016GL068992

Fujimoto, K., & Machida, S. (2006). A generation mechanism of electrostatic waves and subsequent electron heating in the plasma sheet–lobe boundary region during magnetic reconnection. *Journal of Geophysical Research*, *111*, A09216. https://doi.org/10.1029/2005JA011542

Grigorenko, E. E., Zelenyi, L. M., Dolgonosov, M. S., Artemiev, A. V., Owen, C. J., Sauvaud, J.-A., et al. (2011). Non-adiabatic ion acceleration in the Earth magnetotail and its various manifestations in the plasma sheet boundary layer. *Space Science Reviews*, *164*, 133–181. https://doi.org/10.1007/s11214-011-9858-9

Harvey, C. C. (1998). Spatial gradients and the volumetric tensor. *ISSI Science Research Series*, *1*, 307–322.

Lindqvist, P.-A., Olsson, G., Torbert, R. B., King, B., Granoff, M., Rau, D., et al. (2016). The spin-plane double probe electric field instrument for MMS. *Space Science Reviews*, *199*, 137–165. https://doi.org/10.1007/s11214-014-0116-9

Nagai, T., Fujimoto, M., Nakamura, R., Baumjohann, W., Ieda, A., Shinohara, I., et al. (2005). Solar wind control of the radial distance of the magnetic reconnection site in the magnetotail. *Journal of Geophysical Research*, *110*, A09208. https://doi.org/10.1029/2005JA011207

Nakamura, T. K. M., Genestreti, K. J., Liu, Y.-H., Nakamura, R., Teh, W.-L., Hasegawa, H., et al. (2018b). Measurement of the magnetic reconnection rate in the Earth's magnetotail. *Journal of Geophysical Research: Space Physics*, *123*, 9150–9168 https://doi.org/10.1029/2018JA025713

Nakamura, T. K. M., Nakamura, R., Varsani, A., Genestreti, K. J., Baumjohann, W., & Liu, Y.-H. (2018a). Remote sensing of the reconnection electric field from in situ multipoint observations of the separatrix boundary. *Geophysical Research Letters*, *45*, 3829–3837. https://doi.org/10.1029/2018GL078340

Nakamura, R., Varsani, A., Genestreti, K. J., Le Contel, O., Nakamura, T., Baumjohann, W., et al. (2018). Multiscale currents observed by MMS in the flow braking region. *Journal of Geophysical Research: Space Physics*, *123*, 1260. https://doi. org/10.1002/2017JA02468

Onsager, T. G., Thomsen, M. F., Gosling, J. T., & Bame, S. J. (1990). Electron distributions in the plasma sheet boundary layer: Time-of-flight effects. *Geophysical Research Letters*, *11*, 1837–1840.

Parks, G., Chen, L. J., McCarthy, M., Larson, D., Lin, R. P., Phan, T., et al. (1998). New observations of ion beams in the plasma sheet boundary layer. *Geophysical Research Letters*, *25*, 3285. https://doi.org/10.1029/98GL02208

Plaschke, F., Kahr, N., Fischer, D., Nakamura, R., Baumjohann, W., Magnes, W., et al. (2016). Steepening of waves at the duskside magnetopause. *Geophysical Research Letters*, *43*, 7373–7380. https://doi.org/10.1002/2016GL070003

Pollock, J. C., Moore, T., Jacques, A., Burch, J., Gliese, U., Saito, Y., et al. (2016). FPI for the Magnetospheric Multiscale (MMS) Mission. *Space Science Reviews*. https://doi.org/10.1007/s11214-016-0245-4

Russell, C. T., Anderson, B. J., Baumjohann, W., Bromund, K. R., Dearborn, D., Fischer, D., et al. (2016). The Magnetospheric Multiscale Magnetometers. *Space Science Reviews, 199*, 189–256. https://doi.org/10.1007/s11214-014-0057-3

Sauvaud, J.-A., & Kovrazhkin, R. A. (2004). Two types of energy-dispersed ion structures at the plasma sheet boundary. *Journal of Geophysical Research*, *109*, A12213. https://doi.org/10.1029/2003JA010333

Sauvaud, J.-A., Popescu, D., Delcourt, D. C., Parks, G. K., Brittnacher, M., Sergeev, V. A., & Kovrazhkin, R. A. (1999). Sporadic plasma sheet ion injections into the high altitude auroral bulge: Satellite observations. *Journal of Geophysical Research*, *104*, 28. https://doi.org/10.1029/1999JA900293

Sergeev, V. A., Apatenkov, S. V., Angelopoulos, V., McFadden, J. P., Larson, D., Bonnell, J. W., et al. (2008). Simultaneous THEMIS observations in the near-tail portion of the inner and outer plasma sheet flux tubes at substorm onset. *Journal of Geophysical Research*, *113*, A00C02. https://doi.org/10.1029/2008JA013527

Sergeev, V. A., Sauvaud, J.-A., Popescu, D., Kovrazhkin, R. A., Lutsenko, V. N., Zelenyi, L. M., et al. (2000). Plasma sheet ion injections into the auroral bulge: Correlative study of spacecraft and ground observations. *Journal of Geophysical Research*, *105*, 18. https://doi.org/10.1029/1999JA900435

Sergeev, V. A. S. V. A., Nakamura, R., Plaschke, F., Baumjohann, W. E. P., Khotyaintsev, Y., Burch, J. L., et al. (2020). MMS observations of reconnection sepatrix region in the magnetotail at different distances from the active neutral X-line. *Journal of Geophysical Research*, *126*, e2020JA028694. https://doi.org/10.1029/2020JA028694

Shirai, H., Maezawa, K., Fujimoto, M., Mukai, T., Yamamoto, T., Saito, Y., & Kaya, N. (1997). Drop-off of the polar rain flux near the plasma sheet boundary. *Journal of Geophysical Research*, *102*(A2), 2271–2278 https://doi.org/10.1029/96JA02600

Takahashi, K., & Hones, E. W. (1988). ISEE 1 and 2 observations of ion distributions at the plasma sheet-tail lobe boundary. *Journal of Geophysical Research*, *93*, 8558. https://doi.org/10.1029/JA093iA08p08558

Tsyganenko, N. A., & Andreeva, V. A. (2015). A forecasting model of the magnetosphere driven by an optimal solar-wind coupling function. *Journal of Geophysical Research*, *120*, 8401–8425. https://doi.org/10.1002/2015JA021641

Varsani, A., Nakamura, R., Sergeev, V. A., Baumjohann, W., Owen, C. J., Petrukovich, A. A., & Ergun, R. E. (2017). Simultaneous remote observations of intense reconnection effects by DMSP and MMS spacecraft during a storm time substorm. *Journal of Geophysical Research: Space Physics*, *122*, 10891–10909.https://doi. org/10.1002/2017JA024547